Journal of Chromatography, 211 (1981) 313–335
Elsevier Scientific Publishing Company, Amsterdam — Printed in The Netherlands

CHROM. 13,771

COMPUTER SIMULATION AND EXPERIMENTAL VALIDATION OF ISOELECTRIC FOCUSING IN AMPHOLINE-FREE SYSTEMS

M. BIER*, R. A. MOSHER and O. A. PALUSINSKI
Biophysics Technology Laboratory, University of Arizona, Tucson, AZ 85721 (U.S.A.)
(Received March 4th, 1981)

SUMMARY

An abbreviated version of a mathematical model of the steady state in isoelectric focusing is presented. Details of the mathematical transformations leading to a model suitable for computer implementation and numerical solution are given in the Appendix. The model describes the structure of concentration, pH, conductivity and potential gradients arising from the focusing of electrochemically defined ampholytes. Some of the results of computer simulations of two and three component systems are of particular interest to the experimentalist and are presented together with experimental validation of this model.

INTRODUCTION

Isoelectric focusing (IEF) is a powerful separation method first proposed by Kolin[1] and reduced to practice by Svensson[2]. The method has since gained widespread popularity, mainly because of the development by Vesterberg[3] of Ampholine (Tradename of LKB, Bromma, Sweden), a polyaminopolycarboxylic acid buffer mixture produced by random polymerization. The constituents of this mixture migrate electrophoretically to stationary zones in the separation field, thereby establishing a relatively stable "natural" pH gradient.

Ampholine and other similar commercial carrier ampholytes are well suited for analytical purposes, but for preparative applications there are several shortcomings: they result in product contamination with a chemically and biologically ill-defined material; they are rather expensive; and they do not allow for custom-design of pH profiles. Our recent development of a large scale preparative IEF apparatus based on a novel recycling principle[4–6] has prompted us to reexamine the possible development of Ampholine-free buffering systems using chemically defined mixtures.

In the last few years there have been several attempts to develop such buffering systems, using a variety of approaches[7–14]. In particular, Chrambach and his coworkers[7–9] have made many attempts to construct useful pH gradients using various ampholyte mixtures, while others[10–13] have also considered non-amphoteric buffer mixtures. In contrast, Caspers *et al.*[14] have used amino acids and buffers to modulate the pH gradients formed by Ampholine. It was generally appreciated that the quan-

0021-9673/81/0000–0000/$02.50

tities of individual components utilized and their specific characteristics must uniquely determine the shape of the pH gradient established, the sample capacity, and the resolution. It should also be appreciated that most of these approaches were purely empirical and have suffered from the absence of an explicit model demonstrating the contribution of individual components to gradient formation.

It appeared, therefore, that further progress required a better understanding of IEF, *i.e.*, a theory describing the structure of concentration, pH, conductivity and potential gradients generated by focusing a limited number of electrochemically defined ampholytes to the steady state. Unfortunately, the very usefulness of Ampholine has also alleviated the need for the development of such a theory. Most prior theoretical treatments of IEF assumed the preexistence of linear pH and/or conductivity gradients[15,16], a situation fairly approximated if Ampholine is employed. The best model of IEF hitherto available is that of Almgren[17], but it has only partially fulfilled the need, as its simplifying assumptions were too limiting for practical applications.

A suitable detailed theory of IEF has recently been developed by Palusinski *et al.*[18] in a form suitable for computer modeling. In the present paper we wish to report an abbreviated version of the model, limited to two ampholytes, as well as some of the results of computer simulations of IEF which we believe are of particular interest to the experimentalist. In addition, we are presenting some of our laboratory data which validate, at least qualitatively, these computer simulations.

MATERIALS AND METHODS

A DEC-10 processor is used for the maintenance and editing of our programs. All computations are performed on the CYBER 175 processor by transferring the files from DEC-10 on simple commands. The differential equations are solved using DARE P software[19]. The program can readily be implemented on any computer provided with a FORTRAN compiler and will be supplied on request.

The amino acids and peptides used in this work were purchased from Vega Biochemicals (Tucson, AZ, U.S.A.). Other chemicals were purchased from Eastman-Kodak (Rochester, NY, U.S.A.).

Experimental IEF was carried out in three systems: thin-layer polyacrylamide gels, the LKB Model 8101 focusing column, and the recycling IEF apparatus developed in this laboratory[4–6]. Gel pH and concentration profiles were determined by sectioning the polyacrylamide gels in 0.5-cm long segments and elution in 0.01 *M* KCl. Amino acid concentrations were determined using the Durrum automatic amino acid analyzer.

MODEL FORMULATION

A detailed account of our model of the steady state in IEF has been recently presented[18]. Briefly, the treatment considers only simple ampholytes, *i.e.*, it is assumed that only the two apparent dissociation constants (p*K*s) nearest the isoelectric point (p*I*) of an ampholyte influence its behavior in the steady state. The analysis is one-dimensional in a stationary fluid with no electroosmosis and at constant temperature.

At present, we wish to present a simplified version of our model, restricting it to binary mixtures only. The construction of the model rests upon the following basic concepts:

(a) The concentrations of component subspecies are described by equations of chemical equilibria.

(b) In the steady state, a balance exists between the mass transports resulting from electromigration and from diffusion.

(c) Electroneutrality is preserved within the relevant physical dimensions.

In such a system, the conductivity σ is given by

$$\sigma = e \sum_{i=1}^{i=8} z_i^2 w_i n_i \tag{1}$$

where e is the Faraday constant (96,500 Coulombs/mole), z_i valences (dimensionless 0, +1, −1), w_i mobility coefficients ($cm^2/V \cdot sec$), n_i concentrations ($mole/cm^3$). Subscripts 1 and 2 refer to hydrogen and hydroxyl ions, 3 and 6 to the neutral species of ampholytes 1 and 2, respectively, 4 and 7 to the cationic species of the two ampholytes, and 5 and 8 to their anionic species. The mobility coefficients w_i are related to the conventional electrophoretic mobilities μ_i by $\mu_i = w_i z_i$, and to the diffusion constants D_i by the Einstein relation $D_i = RTw_i/e$.

The ampholyte conservation equation is

$$e(w_4 n_4 - w_5 n_5)\frac{d\varphi}{dx} + RT\left(w_3 \cdot \frac{dn_3}{dx} + w_4 \cdot \frac{dn_4}{dx} + w_5 \cdot \frac{dn_5}{dx}\right) = 0 \tag{2a}$$

$$e(w_7 n_7 - w_8 n_8)\frac{d\varphi}{dx} + RT\left(w_6 \cdot \frac{dn_6}{dx} + w_7 \cdot \frac{dn_7}{dx} + w_8 \cdot \frac{dn_8}{dx}\right) = 0 \tag{2b}$$

where φ is the local potential (V), x is the distance (cm), from the anodic end of the column, R is the universal gas constant ($g \cdot cm^2/sec^2$) and T is the absolute temperature (°K).

The conservation of charge equation has the form

$$\sigma \frac{d\varphi}{dx} + RT \sum_{i=1}^{i=8} z_i w_i \frac{dn_i}{dx} = -J \tag{3}$$

where J is the current density (A/cm^2).

In addition to the above differential equations the algebraic relation

$$n_1 - n_2 + n_4 - n_5 + n_7 - n_8 = 0 \tag{4}$$

describes the electroneutrality of the solution.

The chemical equilibria for each ampholyte are described by the usual proton dissociation equations defining the constants K_{11} and K_{12} for the first ampholyte and the constants K_{21} and K_{22} for the second ampholyte.

The above equations are non-linear and cannot be solved analytically. Thus, a numerical approach was necessary, requiring the transformations of equations described in the Appendix. The algebraic equations are used to eliminate all concentration terms except those of the two neutral subspecies, n_3 of the first ampholyte and n_6 of the second ampholyte. These transformations produce

$$\frac{dn_3}{dx} = \frac{J}{RT} \cdot a\,(n_3, n_6)\left(\frac{w_4}{K_{11}} \cdot n_1 - w_5 K_{12} \cdot \frac{1}{n_1}\right) n_3 \tag{5}$$

$$\frac{dn_6}{dx} = \frac{J}{RT} \cdot b\,(n_3, n_6)\left(\frac{w_7}{K_{21}} \cdot n_1 - w_8 K_{22} \cdot \frac{1}{n_1}\right) n_6 \tag{6}$$

which define the profiles of the concentrations of the above two species along the IEF column axis. The functions a and b are defined in the Appendix.

Eqns. 5 and 6 lead to the following important conclusions:

(a) The two factors, the applied current density and the distance over which the gradients are developed, have a reciprocal relationship. The same relative profiles will be obtained as long as the product of column length (x) and applied current density (J) is kept constant. Thus, the voltage needed to obtain full development of the gradients across any column is independent of its length.

(b) The sign of the concentration gradients dn_3/dx and dn_6/dx is determined by the sign of the terms in parenthesis in eqns. 5 and 6, since all other factors are positive. This yields the following inequalities

$$n_1^2 > w_5 K_{12} K_{11}/w_4 \tag{7}$$

$$n_1^2 < w_8 K_{21} K_{22}/w_7 \tag{8}$$

for the growth of n_3 and decrease of n_6. These inequalities explain the concentration maxima reported in Fig. 3.

RESULTS OF SIMULATION STUDIES

The foregoing equations have been suitably transformed for computer implementation, as partially shown in the Appendix, and have been exercised to simulate the IEF process in binary and tertiary mixtures of ampholytes[18]. At present we wish to present some of the simulation studies which are of particular importance for experimental IEF. Our studies comprised modeling with hypothetical ampholytes, to which arbitrary electrochemical parameters were assigned, as well as with real compounds for which literature cited parameters were used. Most simulations have been conducted with binary mixtures, as the rational selection of more complex mixtures requires a prior understanding of the interaction between any two ampholytes focused adjacently in the separation field.

Our model requires the input of the following parameters:

(a) Dimensions of the column: all data to be presented assume a length of 1 cm and a cross-section of 1 cm^2.

(b) The mobility coefficient w of all components of the mixture. Different mobility coefficients can be assigned to the positive, neutral and negative subspecies of each ampholyte, as they may vary by as much as 5% due to the greater hydration of the carboxylate group[20]. Most of the mobility coefficients for real ampholytes were calculated from the diffusion constants given by Longsworth[21] or arrived at by interpolation as a function of molecular volumes[21,22].

(c) The dissociation constants of all components. For ampholytes with more than two dissociating groups, only the constants nearest the pI were used. This results in a negligible error if the remaining dissociation constants differ by more than an order of magnitude from those used.

(d) The initiating (boundary) concentrations of the two ampholytes at any arbitrary point along the column axis.

(e) The applied current density.

The output of a computer simulation is:

(a) The concentration profiles of all subspecies of both ampholytes along the column axis, as well as the total amounts in the column.

(b) The pH, conductivity, and electrical potential profiles along the column axis, as well as other complementary data.

Simulations with hypothetical ampholytes

The assignment of arbitrary electrochemical parameters to hypothetical ampholytes has permitted a systematic evaluation of the effects of the input parameters on simulated IEF.

The data presented in the composite Fig. 1 illustrate the effects of applied current density on the concentration, pH and conductivity profiles obtained on simulated focusing of a binary mixture of ampholytes in the neutral pH region. The input parameters are listed in Table I. The plots labelled A were obtained at the lowest current density, plots labelled B and C at three and nine times higher current densities, respectively. The concentration plots show that the more acidic ampholyte (1) accumulates at the anode, the more basic one (2) accumulating at the cathode, their concentrations decreasing monotonically towards the opposite electrodes. As shown previously[18], the ampholytes are essentially isoelectric at the electrodes, with the proportion of charged species increasing as the total concentration decreases. As a result, the pH curves span the range between the isoelectric points of the two ampholytes (pI 6 and 7, respectively) and the conductivity is maximal in the center of the column, decreasing towards both electrodes. An increase in current density (plots B and C) results in the contraction of the effective distance over which full deployment of gradients is obtained. This is dictated by eqns. 5 and 6 which show that an X-fold increase in current density will result in an equivalent reduction in column length over which full deployment of profiles is obtained. The computer calculated total voltages for the above three systems were 0.43 (A), 1.53 (B), and 4.83 (C). These voltages are substantially lower than voltages customarily applied in IEF using commercial carrier ampholytes. Experimental work, which will be discussed, has confirmed this computer prediction. Thus at high applied potentials, no smooth pH or concentration profiles can be expected, the step-gradients obtained being more reminiscent of isotachophoresis than of IEF.

It should also be pointed out that in the above simulations the total amount of

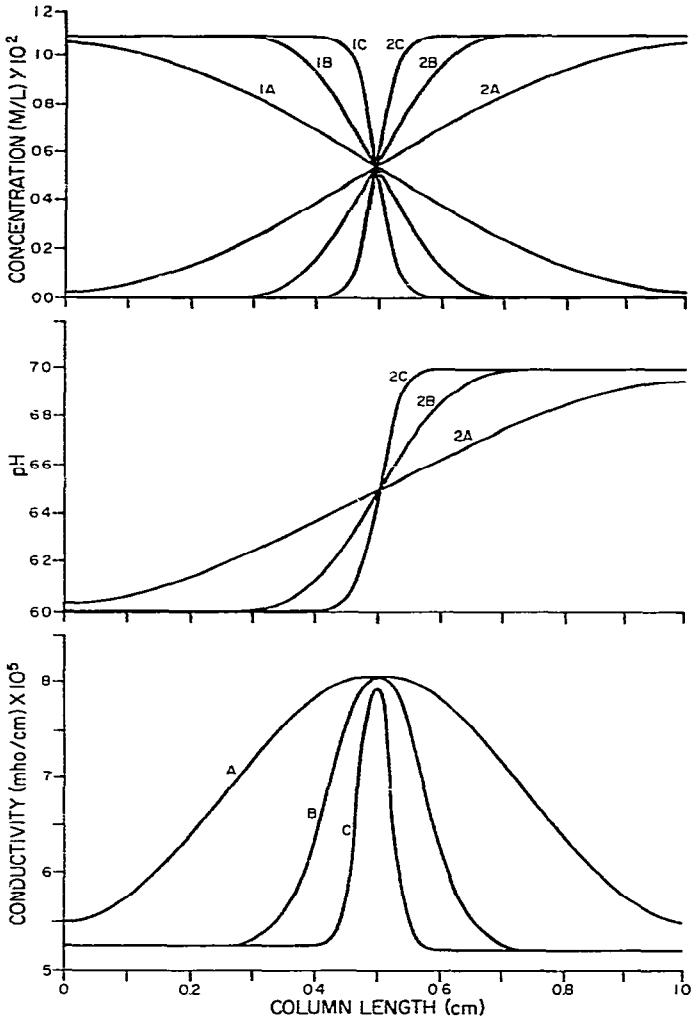

Fig. 1. Effects of current density on computer generated profiles of concentration, pH, and conductivity at the steady state in IEF. Current densities: A, 0.0288 mA/cm^2; B, 0.0864 mA/cm^2; C, 0.2592 mA/cm^2. All other input parameters are listed in Table I.

each ampholyte in the column remains unchanged by the alteration of applied current, since the profiles remain symmetrical. The general shape of the plots shown in Fig. 1 will remain virtually unchanged if concentrations and applied current are varied by the same factor. Total ampholyte content and conductivity will be, of course, proportional to concentration. Similarly, the plots are not changed noticeably if mobility coefficients for both ampholytes and the applied current are altered by the same factor.

In the above plots, all profiles are essentially symmetrical. This is due to the symmetry of the assigned electrochemical parameters and the pH range being close to neutrality. In particular, the mobility coefficients for all subspecies of both ampho-

TABLE I

INPUT ELECTROCHEMICAL PARAMETERS FOR SIMULATIONS REPORTED IN FIGS. 1–4

Figure No.	*Component No.*	pK_1	*pI*	pK_2	*Mobility coefficient* $\times 10^4$		
					Cation	*Neutral*	*Anion*
1	1A–C	5.0	6.0	7.0	3.0	3.0	3.0
	2A–C	6.0	7.0	8.0	3.0	3.0	3.0
2	1D	5.0	6.0	7.0	3.0	3.0	3.0
	2D	6.0	7.0	8.0	3.0	3.0	3.0
	1E	5.0	6.0	7.0	3.15	3.0	2.85
	2E	6.0	7.0	8.0	3.15	3.0	2.85
3–4	1F	1.5	2.5	3.5	3.0	3.0	3.0
	2F	2.5	3.5	4.5	3.0	3.0	3.0
	1G	1.5	2.5	3.5	3.15	3.0	2.85
	2G	2.5	3.5	4.5	3.15	3.0	2.85
	1H	9.5	10.5	11.5	3.0	3.0	3.0
	2H	10.5	11.5	12.5	3.0	3.0	3.0

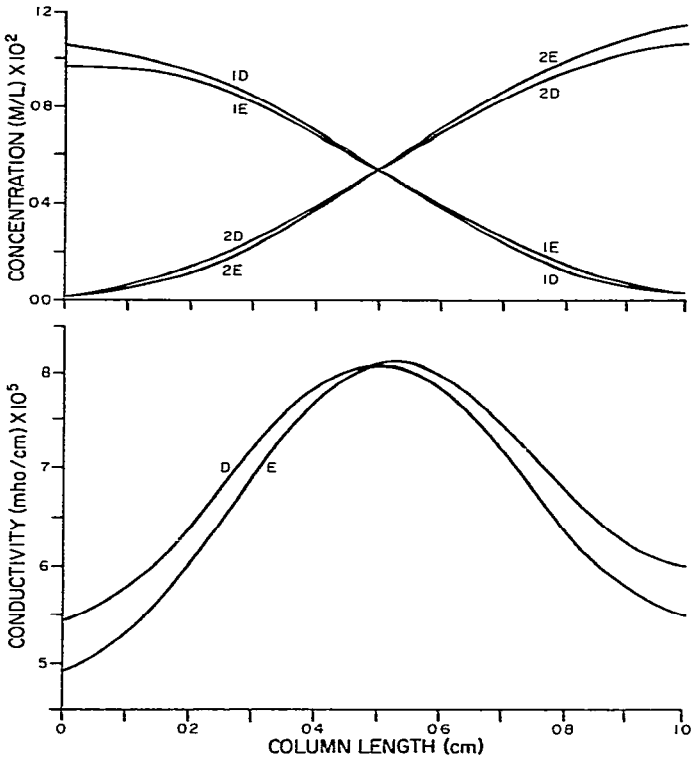

Fig. 2. Effects of differences in mobility coefficients of cationic, neutral and anionic ampholyte species on computer generated profiles of concentration and conductivity in IEF. Current densities were 0.0288 mA/cm² for both systems, all other input parameters being listed in Table I.

lytes were assumed to be identical, which is not the case in actuality. If the cationic subspecies of both ampholytes are assumed to have a higher mobility coefficient than the more hydrated anionic subspecies[20], the profiles are no longer symmetrical, as shown in Fig. 2. The input parameters are presented in Table I. The pH curves were omitted, as they were essentially superimposable.

Symmetry is also lost if the simulation is performed outside of the neutral pH region, due to the contributions of hydrogen or hydroxyl ions to the conductivity. This is illustrated in Fig. 3, which shows the concentration and conductivity plots for binary mixtures similar to those presented in the previous figures, except that they were centered around pH 3 (plot F for components with identical mobility coefficients for all subspecies and plot G where higher cationic mobility coefficients were assigned) and around pH 11 (plot H, with identical mobility coefficients). The simulation input parameters are also listed in Table I. Because of the higher conductivities of these systems significantly higher current densities had to be applied than in the previous simulations.

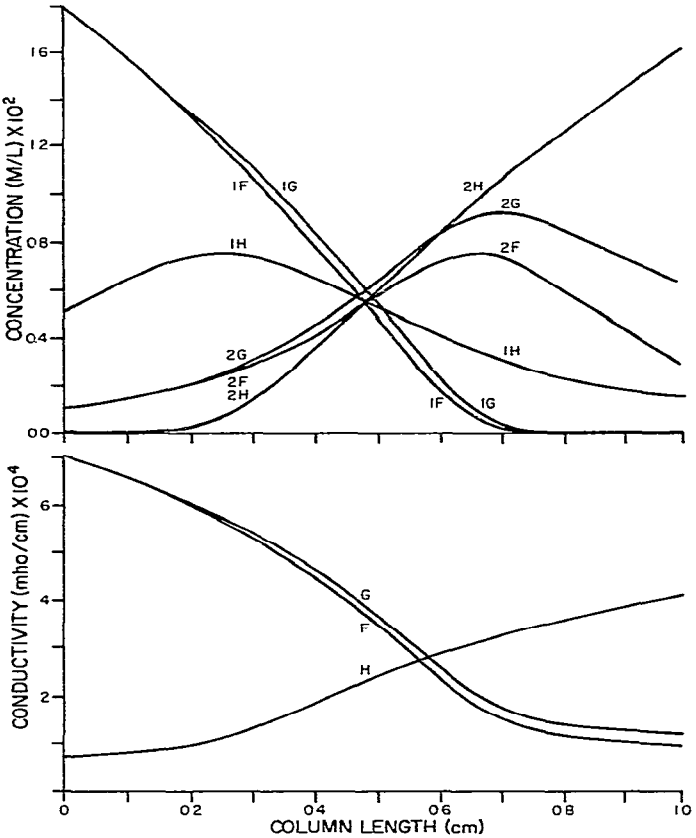

Fig. 3. Effects of low or high pH values on computer generated profiles of concentration and conductivity at the steady state in IEF. Current densities: F and G, 0.20 mA/cm^2; H, 0.10 mA/cm^2. All other parameters are listed in Table I.

The most surprising result of these simulations was that the concentrations of some ampholytes no longer rise monotonically towards the electrodes: at low pH values, the concentration of the more basic ampholytes, 2F and 2G, go through a distinct maximum, while at high pH values the concentration of the more acidic ampholyte, 1H, goes through a maximum. This behavior was quite unexpected, but is explained by the inequalities 7 and 8.

The corresponding pH profiles are given in Fig. 4. It is significant that the pH profiles no longer span the range between the p*I* values of the two constituent ampholytes, but are shifted towards more neutral values. This is in line with the observation of Rilbe[22], who has shown that the pH values of dilute solutions of isoelectric ampholytes do not correspond to their p*I* values (except in the neutral pH region), because of the "buffering action" of water.

In our previous paper[18] we examined the effects of varying the spread between the p*K* values for each ampholyte in binary mixtures, and the effects of varying the

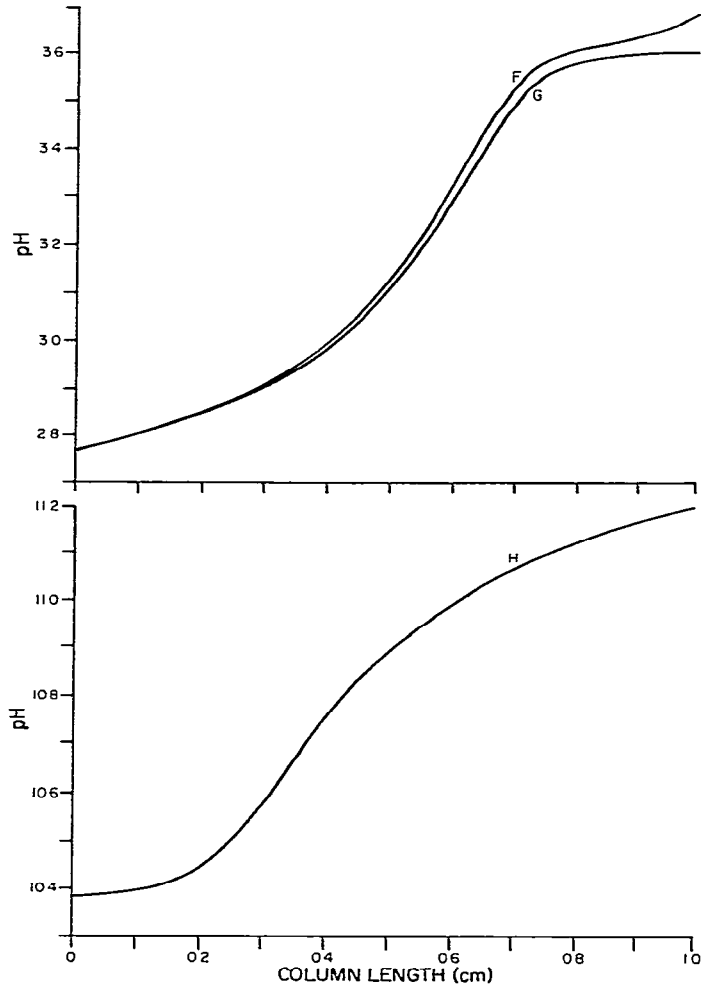

Fig. 4. Computer generated pH profiles corresponding to the simulation data presented in Fig. 3.

spread between the p*I* values of the two components. These simulations were performed in the neutral region, as in acid or alkaline regions the superimposition of the pH effects demonstrated above obscures the results. These pH effects must also be considered if concentrations or mobilities are altered.

The above simulations as well as those previously presented[18] illustrate the effects of the most important experimental variables: the electrochemical properties of the ampholytes (mobility, p*K*, p*I*) and the physical parameters (column dimensions, applied current, and concentrations).

Simulations have also been performed with hypothetical three component systems and will be presented in a future paper. A simulation of a three component system with actual compounds is presented in a following section.

Computer simulations of IEF of real compounds

Following the simulations of IEF of imaginary compounds, the same procedure was applied to real ampholytes. Unfortunately, while hypothetical compounds provide a limitless choice of parameters, there are far fewer actual ampholytes to choose from, *i.e.*, ampholytes for which the required electrochemical parameters have been reported in the literature. The binary systems investigated are listed in Table II. The last column refers to results of the simulation: good refers to systems

TABLE II

INPUT PARAMETERS AND RESULTS OF IEF SIMULATIONS OF REAL AMPHOLYTES

System components	pK_1	pK_2	*ΔpK*	*ΔpI*	*Mobility coefficient* $\times 10^4$	*Current* (mA/cm^2)	*Results*
m-ABA	3.12	4.74	1.62	2.96	3.01	0.16	Aborted
β-Ala	3.6	10.19	6.59		3.63		
m-ABA	3.12	4.74	1.62	0.99	3.01	0.18	Poor
α-Asp-His	3.02	6.82	3.80		2.11		
p-ABA	2.41	4.85	2.44	3.36	3.28	0.24	Aborted
β-Ala	3.60	10.19	6.59		3.63		
p-ABA	2.41	4.85	2.44	2.07	3.28	0.18	Aborted
Tyr-Tyr	3.52	7.68	4.16		1.56		
β-Ala	3.60	10.19	6.59	0.70	3.63	0.36	Poor
His	6.0	9.17	3.17		2.85		
β-Ala-His	6.83	9.51	2.68	2.59	2.30	0.098	Good
Arg	9.04	12.48	3.44		2.71		
β-Ala-His	6.83	9.51	2.68	1.53	2.30	0.108	Good
Orn	8.65	10.76	2.11		3.11		
α-OH-Asn	2.31	7.17	4.86	2.68	2.95	0.08	Good
His-Gly	6.27	8.57	2.30		2.40		
Asp	1.88	3.65	1.90	0.98	2.97	0.40	Good
m-ABA	3.12	4.74	1.62		3.01		

TABLE II *(continued)*

System components	pK_1	pK_2	ΔpK	ΔpI	*Mobility coefficient* $\times 10^4$	*Current* (mA/cm^2)	*Results*
Asp	1.88	3.65	1.90	0.58	2.97	0.80	Conc. max. *p*-ABA
p-ABA	2.41	4.85	2.44		3.28		
Asp	1.88	3.65	1.9	0.28	2.97	0.144	Conc. max. Glu
Glu	2.19	4.25	2.13		3.23		
Asp	1.88	3.65	1.90	2.75	2.97	0.40	Aborted
Gly-Gly	3.15	8.25	5.10		3.08		
α-Asp-His	3.02	6.82	3.80	2.67	2.11	0.079	Good
His	6.0	9.17	3.17		2.85		
α-Asp-His	3.02	6.82	3.80	0.93	2.11	0.25	Fair
Isogln	3.81	7.88	4.07		2.96		
β-Ala-His	6.83	9.51	2.68	1.53	2.30	0.096	Good
Orn	8.65	10.76	2.11		3.11		
Glu	2.19	4.25	1.90	2.47	3.23	0.24	Aborted
Gly-Gly	3.15	8.25	5.10		3.08		
Gly	2.35	9.78	7.43	3.63	4.11	0.10	Good
Orn	8.65	10.76	2.11		3.11		
Gly-Gly	3.15	8.25	5.10	2.47	3.08	0.08	Good
β-Ala-His	6.83	9.51	2.68		2.30		
His	6.0	9.17	3.17	0.58	2.85	0.18	Good
β-Ala-His	6.83	9.51	2.68		2.3		
His	6.0	9.17	3.17	0.30	2.85	0.384	Poor
His-His	6.8	7.8	1.0		1.49		
His	6.0	9.17	3.17	1.09	2.85	0.096	Good
Tyr-Arg	7.55	9.80	2.25		1.58		
His-Gly	5.8	7.82	2.02	1.38	2.4	0.20	Good
β-Ala-His	6.83	9.51	2.68		2.3		
His-His	6.8	7.8	1.0	0.89	2.40	0.30	Fair
β-Ala-His	6.83	9.51	2.68		2.30		
Isogln	3.02	6.82	4.07	1.74	2.96	0.09	Good
His	6.0	9.17	3.17		2.85		
Tri-Gly	3.23	8.09	4.86	1.94	2.59	0.076	Good
His	6.0	9.17	3.17		2.85		
Tyr-Arg	7.55	9.80	2.25	2.08	1.58	0.079	Good
Arg	9.04	12.48	3.44		2.71		
Tyr-Arg	7.55	9.80	2.25	1.02	1.58	0.108	Good
Orn	8.65	10.76	2.11		3.11		
Tyr-Tyr	3.52	7.68	4.16	1.99	1.56	0.06	Good
His	6.0	9.17	3.17		2.85		

where reasonably symmetrical concentration profiles were obtained and reasonably useful pH gradients were projected. Poor refers to concentration profiles which were quite unsymmetrical and where the pH gradients did not appear to be promising. The computer aborted a number of runs, indicating a very unsatisfactory pair, where the concentration of one of the ampholytes reached vanishingly low values. Two systems, aspartic acid–*p*-aminobenzoic acid (Asp/*p*-ABA) and aspartic acid–glutamic acid (Asp/Glu), exhibited concentration maxima of the more basic components (*p*-ABA and Glu, respectively), as were shown for hypothetical compounds in Fig. 3.

To illustrate these results, Fig. 5 shows the quite symmetrical concentration profiles obtained with the aspartic acid–*m*-aminobenzoic acid (Asp/*m*-ABA) system, resulting in a nearly linear pH profile. This can be contrasted with the histidylhistidine–histidine (His-His/His) pair (Fig. 6), which we expected to be an excellent combination, both being "good" ampholytes, *i.e.*, having quite small ΔpK values. The simulation data present grossly unsymmetrical concentration profiles and the pH profile appears to be virtually useless.

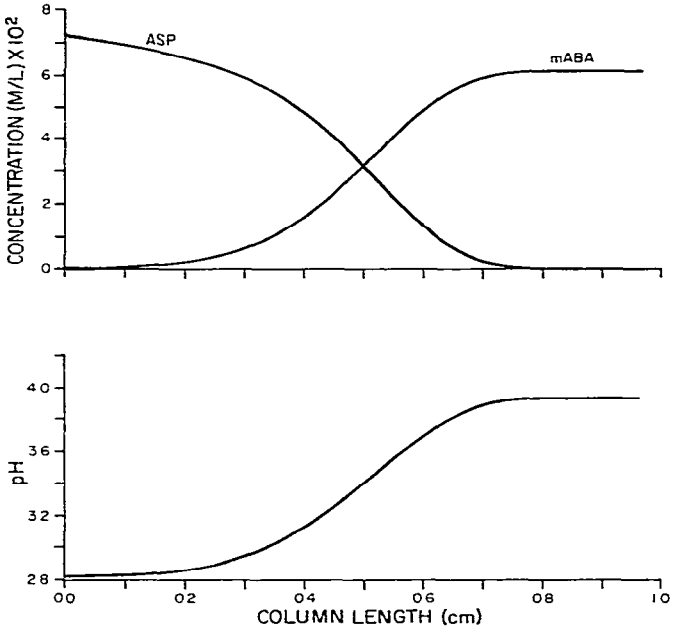

Fig. 5. Computer generated concentration and pH profiles for the focusing of aspartic acid ($pI = 2.95$, $\Delta pK = 1.91$) and *m*-aminobenzoic acid ($pI = 3.93$, $\Delta pK = 1.62$) at a current density of 0.40 mA/cm². The computer calculated voltage across the column was 0.59 V.

Experimental validation of computer simulations

The experimental validation studies were aimed at confirming the two most striking results of the simulations: (i) the low voltages needed to obtain full deployment of the concentration and pH gradients and (ii) the steep gradients obtained at higher voltages.

The existence of the steep gradients was confirmed experimentally in the LKB focusing column, using the system glutamic acid–histidine and the indicator dye

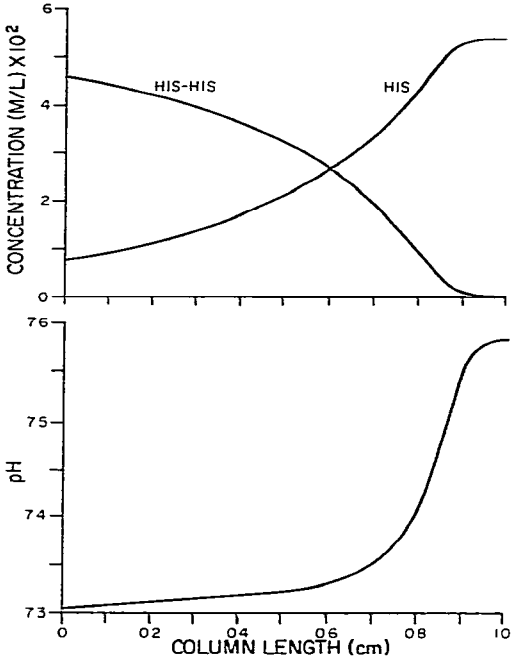

Fig. 6. Computer generated concentration and pH profiles for the focusing of histidylhistidine (pI = 7.3, ΔpK = 1) and histidine (pI = 7.59, ΔpK = 3.17) at a current density of 0.38 mA/cm^2. The computer calculated voltage across the column was 2.4 V.

methyl red as sample. The focusing was carried out at 1000 V, for 43 h. At the end of the focusing, the dye was localized at the center of the column in a narrow band of only 6 mm width, the upper half of the band being yellow and the lower red. Thus, this confirmed the existence of a step pH gradient between pH 3.2 and pH 7.6, which was projected by the simulation.

The validation of focusing obtainable at very low voltages was undertaken using the glycylglycylglycine–histidine (Tri-Gly/His) system. Fig. 7 shows the computer predicted concentration and pH gradients for this system, chosen because it encompasses the pH range where hemoglobin should focus. The model was exercised at the current densities of 0.07 mA/cm^2 and 0.2 mA/cm^2, the computer predicted voltages being 1.3 V and 10 V, respectively.

It was deemed essential to validate the prediction that focusing could be obtained at such low voltages. A sample of porcine hemoglobin was focused in a thin-layer polyacrylamide gel, 5% acrylamide, 0.17% bisacrylamide, 20% glycerol, made 25 mM with respect to Tri-Gly and His. A constant voltage of only 5 V was applied across a distance of 10 cm of the gel, and the focusing was continued for 6 days. The final current density was 0.042 mA/cm^2. The pH gradient was similar to the predicted one, except that it was skewed towards lower pH values, presumably due to the persulfate used as the polymerization catalyst. A photograph of the gel is shown in Fig. 8 and it clearly shows that the bulk of the hemoglobin has focused, leaving a trailing edge, there being two additional rather sharply focused protein bands at lower pH values. This experiment has been repeated a number of times, with quite

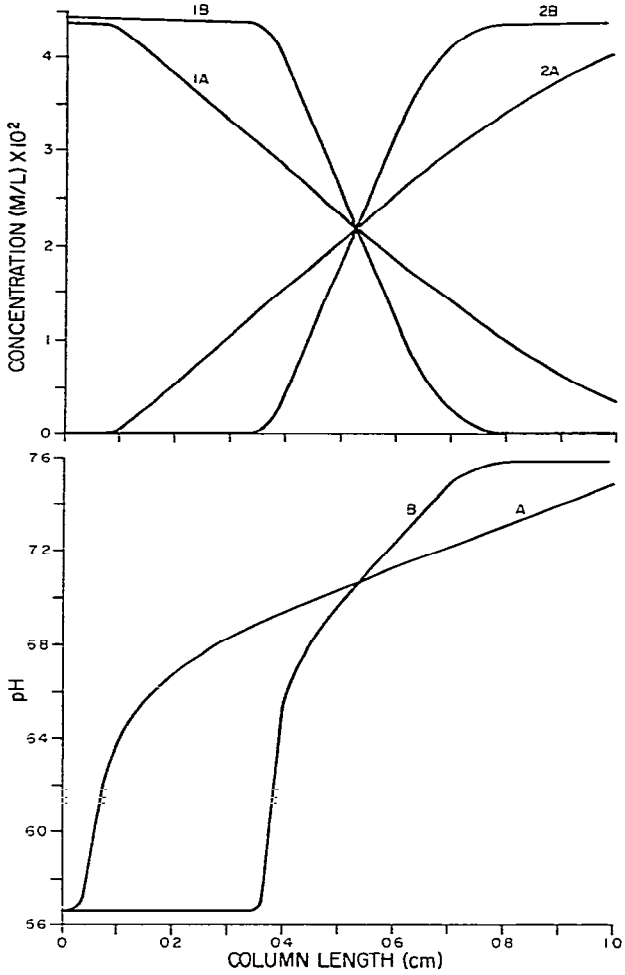

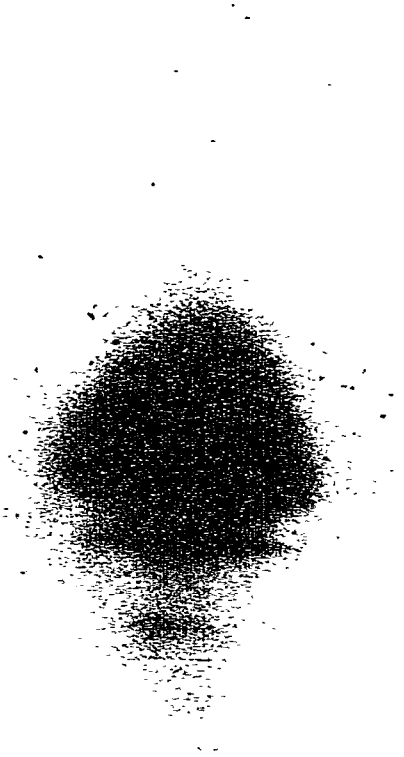

Fig. 7. Computer generated concentration and pH profiles for the focusing of glycylglycylglycine (1A and 1B) (pI = 5.65, ΔpK = 4.86) and histidine (2A and 2B) (pI = 7.59, ΔpK = 3.17). Current densities: A, 0.07 mA/cm² at 1.2 V; B, 0.20 mA/cm² at 10.1 V.

Fig. 8. Photograph of the focused pattern of a sample of porcine hemoglobin in a polyacrylamide gel. The pH gradient was established using 25 mM each of glycylglycylglycine and histidine. Focusing was carried out for 6 days at a potential of 5 V across 10 cm of the gel. The anode is at the bottom.

similar results. Analysis of the distribution of the two components, Tri-Gly and His, has shown that their concentrations overlap at such low voltages, as predicted in plot A of Fig. 7, but are nearly completely separated at voltages higher than roughly 20 V.

The simulation of a three-component system, glutamic acid–cycloserine–histidine (Glu/C-Ser/His), is shown in Fig. 9. The concentration profiles show that the two end components (Glu and His) are widely separated by a non-Gaussian zone of C-Ser. It should be pointed out that the concentration of C-Ser in this zone is not constant, but decreases slightly from glutamic acid to histidine. The pH profile shows two steep pH gradients due to the interactions of Glu/C-Ser and C-Ser/His, respec-

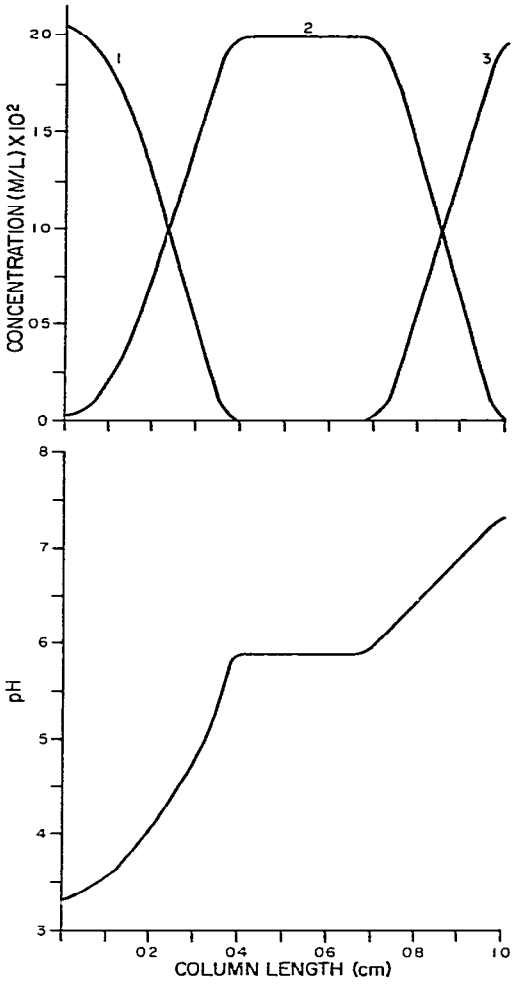

Fig. 9. Computer generated concentration and pH profiles for the three-component mixture of glutamic acid (1) (pI = 3.23, ΔpK = 2.13), cycloserine (2) (pI = 5.90, ΔpK = 3.0), and histidine (3) (pI = 7.59, ΔpK = 3.17) at a current density of 0.13 mA/cm^2 and a potential of 1.8 V.

tively. The conductivity profile, not displayed, exhibits two peaks, corresponding to the two steep pH gradients, separated by a "conductivity gap" due to C-Ser. Such a system was expected to resolve any two proteins with pI values on either side of the C-Ser generated pH plateau. This has been verified in polyacrylamide gels, the LKB focusing column and the recycling IEF apparatus[4–6] developed in our laboratory. Fig. 10 shows the separation of bromophenol blue-stained albumin and red hemoglobin in the recycling apparatus. With all three methods excellent focusing of the two proteins was obtained, the blue albumin focusing in the Glu/C-Ser pH gradient, and the red hemoglobin in the C-Ser/His pH gradient. In the recycling IEF apparatus, the same final protein distribution was obtained whether the albumin and hemoglobin were added as a mixed sample or whether their relative initial applications were

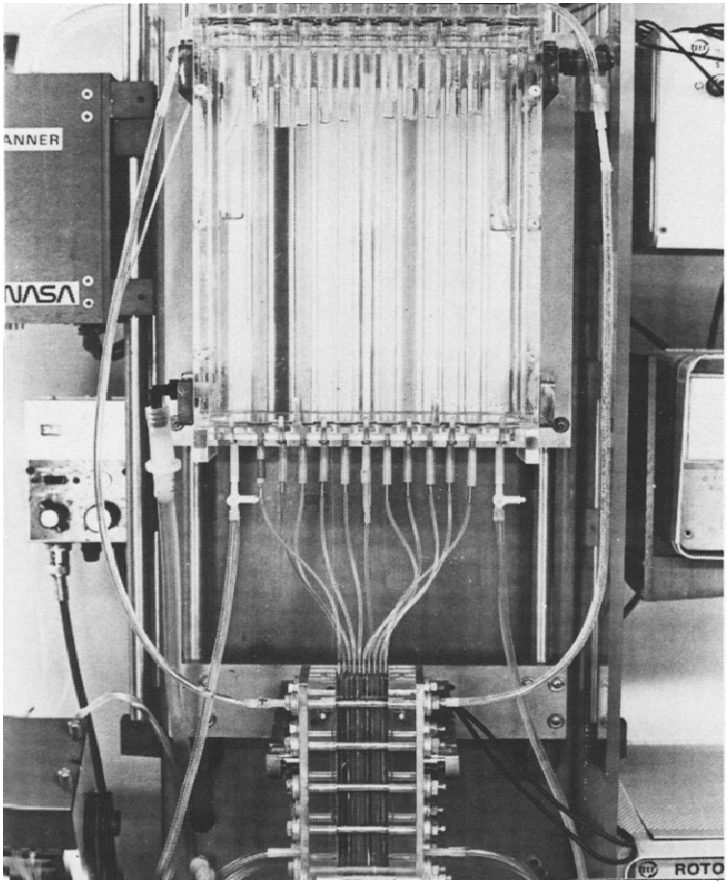

Fig. 10. Photograph of the preparative separation of 500 mg each of porcine hemoglobin (pI = 7.4) and human serum albumin (pI = 4.8) in the recycling isoelectric focusing apparatus (for its description see refs. 4–6). The pH gradient was established using the system modeled in Fig. 9, containing 10 mM each of glutamic acid, cycloserine and histidine. The photograph shows the ten-channel heat exchange reservoir at the top and the focusing cell at the bottom. The mixed sample was added to channel 5 of the heat exchanger at the time of current application. The separation was complete in 1 h, with a final focusing voltage of 300 V. Hemoglobin focused mainly in channel 2 (from the cathode), with trace amounts in adjacent channels, and albumin in channel 7 of the heat exchanger. The albumin was visualized by the addition of a small amount of bromophenol blue dye.

reversed with regard to their final position, *i.e.*, the albumin was applied in the channel where hemoglobin was finally focused and *vice versa*. It is significant, however, that this was obtained only if the proteins were added initially, before the ampholytes were focused. Once the pH gradient was formed, no migration of added samples was obtained, due to the conductivity gap. This separation is controlled by the pI of C-Ser (pI = 5.9), which can be replaced by any other ampholyte with similar characteristics. In fact, comparable separation of the above two proteins was obtained with Gly-Gly (pI = 5.7) or with Gly-Gly-Gly (pI = 5.65) replacing C-Ser.

DISCUSSION

The mathematical model of IEF presented in this and the previous paper[18] was developed in the hope that it would be of value in the design of experimental buffer systems using chemically defined components, thus eliminating the need for the ill-defined commercial carrier ampholytes (Ampholine, etc.) in preparative applications. The experimental data presented here have validated, at least qualitatively, the predictions of the computer simulations. These simulations have been carried out only for two- and three-component systems, as more complex mixtures may be constructed only when the interaction between adjacent pairs of ampholytes is understood.

Some general conclusions can be drawn about the relationships between simulation input parameters and output data. These are summarized in Table III, where a value of 1 is assigned to all "standard" input and output data, and the independently varied parameters are in italics. Each horizontal row of the table summarizes the effects, if any, of the change of the underlined input parameter on the other parameters.

TABLE III

COMPUTER PREDICTED EFFECTS OF INPUT PARAMETERS IN FOCUSING

Computer input parameters				*Computer output data*			
Current	*Column length*	*Mobility coefficient*	*Initiating concn.**	*Voltage gradient*	*Total volts*	*Conductivity gradient*	*Total amount*
2	1	1	1	1	1	1	1
1	*2*	1	1	1/2	1	1	2
1	1	*1/2*	1	1	1	1/2	1
1	1	1	*1/2*	1	1	1/2	1/2

* Initiating concentrations are assigned at the midpoint of the column, where the concentration profiles of the two ampholytes are made to intersect.

For example, lines 1 and 2 indicate that reducing the applied current by half requires doubling the column length to obtain identical profiles, with the exception of the voltage gradient profile, which is halved. The longer column will contain twice the total amount of ampholytes, however, the total voltage required is the same. This holds true for all pH regions.

Similarly, line 3 indicates that reducing the mobility factor by half will reduce the conductivity by nearly the same amount. Thus, half the current will be needed for equivalent gradient deployment. Line 4 indicates that halving the initial concentration of both ampholytes will produce the same effect on the profiles as halving the mobility factor, except that it reduces the total ampholyte content of the column. These two relationships hold true only in the neutral pH region. The further from neutrality, the greater the differences in profiles obtained, due to the contributions of hydrogen and hydroxyl ions to the conductivity, as shown in Fig. 3.

In addition, the following conclusions may help in the selection of ampholytes. The most important factors to be considered are the spread between the p*I* values

(ΔpI) of the two ampholytes, and the spread between the pK values (ΔpK) for each ampholyte:

(1) In the neutral pH region, the pH gradient will cover the span between the pI values of the two components[18]. In acidic or alkaline pH ranges, there will be a shift towards neutrality, as shown in Fig. 3.

(2) Quite similar concentration and pH profiles will be obtained at constant ΔpI, irrespective of the ΔpK values of the individual components[18]. However, the greater the ΔpK, the lower the buffering of the system.

(3) Any ionizable group will buffer only within one pH unit of its dissociation constant. Thus, in a two component mixture only the basic group (pK_{12}) of the more acidic component and the acid group (pK_{21}) of the more basic component may exert a buffering action within the established pH gradient.

All of the above three factors should be considered in the selection of components, the optimum being the smallest possible ΔpI and ΔpK values which provide buffering in the desired pH region.

The most surprising outcome of the simulations is the low current density and, therefore, low voltage needed to obtain full gradient deployment, irrespective of column length. These low voltages are sufficient to cause the focusing of proteins, but only with impractically long focusing times. The application of reasonable potentials appears to require on the order of five components per centimeter of column length, as first suggested by Almgren[17]. With fewer components, and at the high potentials usually used in IEF with commercial carrier ampholytes, step-gradients will be obtained, which are more reminiscent of isotachophoresis[23,24] than of IEF. The similarity with isotachophoresis is also shown in the concentration plots in the three component system shown in Fig. 9. The concentration profile of the intermediate component, C-Ser is not Gaussian, but presents a "square" profile, typical of isotachophoresis.

In conclusion, it would appear that for analytical purposes, where nearly linear gradients spanning a relatively broad pH range are desired, custom designed mixtures of the type discussed do not seem to be promising. A great number of components would be required, some of which would certainly be prohibitively expensive. Thus, Ampholine and other similar commercial carrier ampholytes, remain the buffering agent of choice.

For preparative purposes high voltages are important to minimize the focusing time and maximize the resolution. Any separations will be dependent on finding appropriate "spacer" ampholytes with the desired electrochemical properties, primarily the right pI value. The similarity with isotachophoresis is again evident, except that selecting spacers is easier in isotachophoresis, where the net mobilities can be modified by pH adjustment, whereas the pI values of ampholytes are fixed. Nevertheless, the usefulness of simple ampholyte mixtures for preparative purposes was demonstrated by our separation of albumin from hemoglobin, using the three component system Glu/C-Ser/His. While this is an admittedly simple separation, in a subsequent paper we will report the separation of human hemoglobins A and C, using leucylhistidine as the spacer and C-Ser and Lys as terminal components.

APPENDIX

Basic transformation relations

The equations describing the chemical equilibria

$$K_{11} = n_1 n_3/n_4 \qquad K_{12} = n_1 n_5/n_3$$

and

$$K_{21} = n_1 n_6/n_7 \qquad K_{22} = n_1 n_8/n_6$$

for the first and second ampholyte respectively, together with the well-known water dissociation constant $K_w = n_1 n_2$ and the electroneutrality eqn. 4 (see text) form a system of algebraic equations which can be used to express the variables n_1, n_2, n_4, n_5, n_7 and n_8 in terms of n_3 and n_6, which represent the concentration of the uncharged species. Solving these equations by simple elimination we obtain

$$n_1 = \left(\frac{K_w + K_{12} n_3 + K_{22} n_6}{1 + (n_3/K_{11}) + (n_6/K_{21})} \right)^{\frac{1}{2}} \tag{A1}$$

and

$$n_2 = K_w/n_1 \tag{A2}$$
$$n_4 = n_1 n_3/K_{11} \tag{A3}$$
$$n_5 = K_{12} n_3/n_1 \tag{A4}$$
$$n_7 = n_1 n_6/K_{21} \tag{A5}$$
$$n_8 = K_{22} n_6/n_1 \tag{A6}$$

The variable n_1 was not eliminated to simplify the writing. The relations A1–A6 are used to eliminate all variables except n_3 and n_6 in differential eqns. 2 and 3 (see text). These equations contain the derivatives of all variables, therefore the same elimination must be performed with respect to all of these derivatives, with the exception of dn_3/dx and dn_6/dx.

Using eqn. A1 it is derived

$$\frac{dn_1}{dx} = A_1 \cdot \frac{dn_3}{dx} + A_2 \cdot \frac{dn_6}{dx} \tag{A7}$$

where $A_1 = \bar{A_1} A$ and $A_2 = \bar{A_2} A$.

The symbols A, $\bar{A_1}$ and $\bar{A_2}$ represent the following quantities:

$$A = \tfrac{1}{2} \left[K_{11} K_{21} / (K_{12} n_3 + K_{22} n_6 + K_w) (K_{21} n_3 + K_{11} n_6 + K_{11} K_{21})^3 \right]^{\frac{1}{2}} \tag{A8}$$

$$\bar{A_1} = K_{12} K_{11} (n_6 + K_{21}) - K_{21} (K_{22} n_6 + K_w) \tag{A9}$$

$$\bar{A_2} = K_{22} K_{21} (n_3 + K_{11}) - K_{11} (K_{12} n_3 + K_w) \tag{A10}$$

Analogously from eqns. A2–A6 it is derived:

$$\frac{dn_2}{dx} = -\frac{K_w}{n_1^2}\cdot A_1\cdot\frac{dn_3}{dx} - A_2\cdot\frac{K_w}{n_1^2}\cdot\frac{dn_6}{dx} \tag{A11}$$

$$\frac{dn_4}{dx} = \frac{1}{K_{11}}(n_3A_1 + n_1)\frac{dn_3}{dx} + \frac{1}{K_{11}}\cdot n_3A_2\cdot\frac{dn_6}{dx} \tag{A12}$$

$$\frac{dn_5}{dx} = \frac{K_{12}}{n_1}\left(1 - \frac{n_3}{n_1}\cdot A_1\right)\frac{dn_3}{dx} - \frac{K_{12}n_3}{n_1^2}\cdot A_2\cdot\frac{dn_6}{dx} \tag{A13}$$

$$\frac{dn_7}{dx} = \frac{n_6}{K_{21}}\cdot A_1\cdot\frac{dn_3}{dx} + \frac{1}{K_{21}}(n_6A_2 + n_1)\frac{dn_6}{dx} \tag{A14}$$

$$\frac{dn_8}{dx} = -\frac{K_{22}n_6}{n_1^2}\cdot A_1\cdot\frac{dn_3}{dx} + \frac{K_{22}}{n_1}\left(1 - \frac{n_6}{n_1}\cdot A_2\right)\frac{dn_6}{dx} \tag{A15}$$

Transformation of model equations

Conservation of charge. We shall use the notation:

$$\kappa = \sum_{i=1}^{8} z_i^2 w_i n_i \tag{A16}$$

Note that the conductivity, s, can be expressed by $s = e\kappa$. Using eqns. A1–A15 in eqn. 3 results (after some manipulations) in

$$\frac{e}{RT}\cdot\frac{d\varphi}{dx} = -\frac{J}{RT}\cdot\frac{1}{\kappa} - C_1\cdot\frac{dn_3}{dx} - C_2\cdot\frac{dn_6}{dx} \tag{A17}$$

where:

$$C_1 = A_1\cdot\frac{1}{n_1} + \frac{1}{\kappa}\left(\frac{w_4}{K_{11}}\cdot n_1 - \frac{w_5K_{12}}{n_1}\right)$$

$$C_2 = A_2\cdot\frac{1}{n_1} + \frac{1}{\kappa}\left(\frac{w_7}{K_{21}}\cdot n_1 - \frac{w_8K_{22}}{n_1}\right)$$

Conservation of ampholytes. The eqns. 2a and 2b are divided by RT, then A17 is used to eliminate $(e/RT)\,(d\varphi/dx)$. Using eqns. A2–A6 and A11–A15 to eliminate n_4, n_5, n_7, n_8 and their derivatives we obtain (after some manipulations)

$$a_{11}\cdot\frac{dn_3}{dx} - a_{12}\cdot\frac{dn_6}{dx} = \frac{J}{RT}\cdot\frac{B_{11}}{\kappa} \tag{A18}$$

$$-a_{21}\cdot\frac{dn_3}{dx} + a_{22}\cdot\frac{dn_6}{dx} = \frac{J}{RT}\cdot B_{21} \tag{A19}$$

where:

$$a_{11} = w_3 + \frac{w_4}{K_{11}} \cdot \dot{n}_1 + \frac{w_5 K_{12}}{n_1} - \frac{B_{11}^2}{\kappa} \cdot \frac{1}{n_3}$$

$$a_{12} = \frac{B_{11} B_{21}}{\kappa} \cdot \frac{1}{n_6}$$

$$a_{21} = \frac{B_{11} B_{21}}{\kappa} \cdot \frac{1}{n_3}$$

$$a_{22} = w_6 + \frac{w_7}{K_{21}} \cdot n_1 + \frac{w_8 K_{22}}{n_1} - \frac{B_{21}^2}{\kappa} \cdot \frac{1}{n_6}$$

$$B_{11} = \left(\frac{w_4}{K_{11}} - \frac{w_5 K_{12}}{n_1^2} \right) n_1 n_3$$

$$B_{21} = \left(\frac{w_7}{K_{21}} - w_8 K_{22} \cdot \frac{1}{n_1^2} \right) n_1 n_6$$

In order to obtain eqns. 5 and 6, it is necessary to invert the matrix A with non-linear entries a_{ij}. This is possible only when the matrix A is non-singular, *i.e.*, when its determinant is non-zero.

Matrix inversion and determinant computation. It is shown below that the determinant of matrix A (det A) is non-zero, therefore eqns. A18 and A19 can be presented in the form:

$$\frac{\mathrm{d}n_3}{\mathrm{d}x} = \frac{J}{RT} \cdot \frac{B_{11} a_{22} + B_{21} a_{12}}{\kappa \det A} \tag{A20}$$

$$\frac{\mathrm{d}n_6}{\mathrm{d}x} = \frac{J}{RT} \cdot \frac{a_{11} B_{21} + a_{21} B_{11}}{\kappa \det A} \tag{A21}$$

Taking into account the definitions of symbols and the expression for (κ det A) computed below, the eqns. A20 and A21 are transformed easily to forms 5 and 6, where:

$$a(n_3, n_6) = \frac{w_6 + (w_7 n_1 / K_{21}) + (w_8 K_{22} / n_1)}{\kappa \det A}$$

$$b(n_3, n_6) = \frac{w_3 + (w_4 n_1 / K_{11}) + (w_5 K_{12} / n_1)}{\kappa \det A}$$

Determinant computation. In order to simplify the manipulations we introduce the notation:

$$\begin{aligned} w_4 n_1/K_{11} &= p \qquad & w_8 K_{22}/n_1 &= s \\ w_5 K_{12}/n_1 &= q \qquad & w_1 n_1 + w_2 K_w/n_1 &= t \\ w_7 n_1/K_{21} &= r \end{aligned} \tag{A22}$$

Using eqns. A1–A6 in A16 and taking into account that $z_i = 1$ ($i = 1, 4, 7$), -1 ($i = 2, 5, 8$), 0 ($i = 3, 6$) we obtain

$$\kappa = w_1 n_1 + w_2 K_w \cdot \frac{1}{n_1} + \frac{w_4}{K_{11}} \cdot n_1 n_3 + w_5 K_{12} \cdot \frac{n_3}{n_1} + \frac{w_7}{K_{21}} \cdot n_1 n_6 + w_8 K_{22} \cdot \frac{n_6}{n_1} \tag{A23}$$

and using A22 we can write:

$$\kappa = t + (p + q) n_3 + (r + s) n_6$$

Using the definitions of a_{ij} (A18, A19) the determinant of matrix A (det $A = a_{11}a_{22} - a_{12}a_{21}$) can be computed and taking into account A22 expressed in the form:

$$\det A = (w_3 + p + q)(w_6 + r + s) - (w_3 + p + q)(r - s)^2 n_6 \cdot \frac{1}{\kappa} - (w_6 + r + s)(p - q)^2 n_3 \cdot \frac{1}{\kappa}$$

Using eqn. A23 and the above, the following expression results

$$\kappa \det A = (w_3 + p + q)[t(w_6 + r + s) + (r + s) n_6 w_6 + 4rsn_6] + (w_6 + r + s)[(p + q) n_3 w_3 + 4pqn_3]$$

which is needed in the eqns. A20 and A21. It also demonstrates that the determinant is not zero, since κ is positive.

ACKNOWLEDGEMENTS

The authors wish to acknowledge the contribution of Dudley A. Saville of Princeton University to the development of the mathematical model used in the present studies. Supported in part by the NASA Grant NSG-7333 and the NASA Contract NAS8-32950.

REFERENCES

1 A. Kolin, *J. Chem. Phys.*, 22 (1954) 1628.
2 H. Svensson, *Acta Chem. Scand.*, 15 (1961) 325.
3 O. Vesterberg, *Acta Chem. Scand.*, 23 (1969) 2653.
4 M. Bier and N. B. Egen, in H. Haglund, J. G. Westerfeld and J. T. Ball (Editors), *Electrofocus '78*, Elsevier, Amsterdam, 1979, p. 35.
5 N. B. Egen, G. E. Twitty and M. Bier, *17th Aerospace Sciences Meeting, Amer. Inst. Aeronautics and Astronautics, New Orleans, LA, 1979*, Paper No. 79-0405.
6 M. Bier, N. B. Egen, T. T. Allgyer, G. E. Twitty and R. A. Mosher, in E. Gross and J. Meienhofer (Editors), *Peptides Structure and Biological Function*, Pierce, Rockford, IL, 1979, p. 79.
7 A. Chrambach and N. Y. Nguyen, in B. J. Radola and D. Graesslin (Editors), *Electrofocusing and Isotachophoresis*, W. de Gruyter, Berlin, 1977, p. 51.
8 N. Y. Nguyen and A. Chrambach, *Anal. Biochem.*, 74 (1976) 145.
9 N. Y. Nguyen and A. Chrambach, *Anal. Biochem.*, 79 (1977) 462.
10 R. L. Prestidge and M. T. W. Hearn, *Anal. Biochem.*, 97 (1977) 95.
11 R. C. Boltz, T. Y. Miller, P. Todd and N. E. Kukulinsky in A. Chrambach (Editor), *Electrophoresis '78*, Elsevier/North-Holland, Amsterdam, 1978, p. 345.
12 P. Lundahl and S. Hjerten, *Ann. N.Y. Acad. Sci.*, 209 (1973) 94.
13 A. J. P. Martin and F. Hampson, *J. Chromatogr.*, 159 (1978) 101.
14 M. L. Caspers, Y. Posey and R. K. Brown, *Anal. Biochem.*, 79 (1977) 166.
15 S. K. Park, D. J. Cox, D. I. Stimpson and J. R. Cann, *Biophys. Chem.*, 7 (1978) 367.
16 G. H. Weiss, N. Catsimpoolas and D. Rodbard, *Arch. Biochem. Biophys.*, 163 (1974) 106.
17 M. Almgren, *Chemica Scripta*, 1 (1971) 69.
18 O. A. Palusinski, T. T. Allgyer, R. A. Mosher, M. Bier and D. A. Saville, *Biophys. Chem.*, in press.
19 G. A. Korn and J. C. Wait, *Digital Continuous System Simulation*, Prentice-Hall, Englewood Cliffs, NJ, 1978.
20 J. T. Edward and D. Waldron-Edward, *J. Chromatogr.*, 20 (1965) 563.
21 L. G. Longsworth, *J. Amer. Chem. Soc.*, 75 (1953) 5705.
22 H. Rilbe, in N. Catsimpoolas (Editor), *Isoelectric Focusing*, Academic Press, New York, 1976, p. 13.
23 A. Kopwillem, W. G. Merriman, R. M. Cuddeback, A. J. K. Smolka and M. Bier, *J. Chromatogr.*, 118 (1976) 35.
24 M. Bier and T. T. Allgyer, in P. G. Righetti, C. J. van Oss and J. W. Vanderhoff (Editors), *Electrokinetic Separation Methods*, Elsevier/North-Holland, Amsterdam, 1979, p. 450.